A New Depositional Framework for Massive Iron Formations after The Great Oxidation Event

Athena Eyster[1], Latisha Brengman[2], Claire I. O. Nichols[1], Zoe Levitt[1], and Kristin Bergmann[1]

[1]Department of Earth, Atmospheric and Planetary Sciences, Massachusetts Institute of Technology, 77 Massachusetts Avenue, Cambridge, Massachusetts 02139, USA

[2]Department of Earth and Environmental Sciences, University of Minnesota Duluth, 1114 Kirby Drive, Duluth, MN 55812, USA

Corresponding author: Athena Eyster (aeyster@mit.edu)

Key Points:

- Depositional settings and conditions that led to massive iron formations (IF) are complex, yet crucial for interpreting Earth's evolution.
- To determine the context and trigger for the 1.88 Ga resurgence of massive IF, we combine new mapping, stratigraphic and facies datasets.
- These datasets support syn-sedimentary faulting and suggest IF may be linked to oxygen variations, not transgressions or local volcanism.

Abstract

The oldest recognized proxies for low atmospheric oxygen are massive iron-rich deposits. Following the rise of oxygen ~2.4 billion years ago, massive iron formations largely disappear from the geologic record, only to reappear in a pulse ~1.88 Ga, which has been attributed to passive margin transgressions, changing ocean chemistry triggered by intense volcanism, or lowered atmospheric oxygen levels. The North American Gogebic Range has exposures of both volcanics and iron formation, providing an ideal field locality to interrogate the relationship between the lithologies and investigate triggers for this pulse of iron formation. To determine the environmental context and key factors driving post-GOE iron formation deposition, we made detailed observations of the stratigraphy and facies relationships and present updated mapping relationships of the Gogebic Range Ironwood Iron Formation and the Emperor Volcanics. This work expands existing mine datasets and logs to constrain variations in stratigraphy. Our results are the first to quantitatively constrain thickness variations along the entire Gogebic range and tie them to syn-sedimentary faulting along listric normal faults and half grabens. Furthermore, our datasets suggest that initiation of major local volcanism does not coincide with iron formation deposition, thus, local intense volcanism cannot be invoked as a causal trigger. Finally, the possibility of iron formation deposition in a shallow water environment suggests that the post-GOE iron formation pulse may not reflect global marine transgressions, but instead a chemocline shallowing due to decreased atmospheric oxygen.

Plain Language summary

What can massive iron rich rocks tell us about ancient global oxygen levels? Although these rocks have long been recognized as proxies for low oxygen, much is yet to be learnt about the environments that lead to their deposition. These uncertainties are particularly apparent at a time

1.88 billion years ago, when, after atmospheric oxygen rose, there was a renewed peak in the appearance of iron-rich rocks. Was this iron deposition externally triggered by changing global oxygen levels or ocean chemistry linked to intense volcanism? Or does their resurgence represent internal ocean dynamics related to sea level? We present refined relationships of the volcanic and iron-rich rocks in the Lake Superior region, and tie variations to early tectonic activity. The data suggests that the iron deposition onset does not appear to be triggered by local volcanism or sea-level variations, but instead related to decreased oxygen.

1. Introduction

Abundant global oxygen is crucial for macroscopic life on Earth today, yet the tempos and triggers of ancient oxygenation are unknown. Iron formations (originally defined as rocks with >15 wt. % iron) hold important clues to the early evolution of Earth's atmosphere and biosphere, yet questions about their genesis remain. In particular, 1) are all massive iron formations deposited in broadly similar depositional and geochemical settings, and 2) what drives their episodic deposition? The purpose of this study is to assess these questions with a coupled facies-based sedimentological and stratigraphic approaches for the ca. 1.88 Ga Gogebic range exposed near Lake Superior, USA (Michigan-Wisconsin).

Massive iron formations (~10^6 Gtons) occur only in the Precambrian (e.g. Bekker et al., 2014; Konhauser, 2017). When examining the geologic record, the largest volumes of preserved iron formations span the Late Archean to Paleoproterozoic, ending rather abruptly after 1.87 Ga (Gole and Klein, 1981; Trendall, 2002; age from Fralick et al., 2002). This record could reflect continuous iron formation deposition that is no longer evident due to preservation bias, or cessation of massive iron formation deposition after the Great Oxidation Event (GOE) followed by brief iron formation resurgence ca. 1.88 Ga (e.g. Johnson and Molnar, 2019; Konhauser et al., 2017; Bekker et al., 2014; Lyons et al., 2014).

Most agree that iron formations are linked to low atmospheric and dissolved oxygen conditions (Planavsky et al., 2011; Bekker et al., 2010; Klein, 2005). Yet, this is only one of several requirements for their deposition (see Konhauser et al., 2017 for a thorough review). First, anoxic water conditions (<1 mM dissolved oxygen) are required for ferrous iron (Fe^{2+}) to accumulate. There also needs to be a Fe^{2+} source, either from weathered continental material, or hydrothermal/magmatic material introduced directly into the water column. These prerequisites are crucial for accumulating massive volumes of iron. Finally, the iron needs to precipitate out of solution in order to be deposited as sediment. This can happen two ways, via oxidation of Fe^{2+} to Fe^{3+} (the classically proposed model), or via direct precipitation of iron silicates or green rust (e.g. Tosca et al., 2015; Rasmussen et al., 2016; Halevy et al., 2017; Johnson et al., 2018). The first mechanism could occur via oxygenic or anoxygenic photosynthesis, mixing of anoxic ferruginous waters with oxic surface waters at the chemocline, or during storms which bring oxidized surface water into contact with deeper ferruginous waters (Bekker et al., 2014; Posth et al., 2013; Konhauser et al., 2002; Simonson and Hassler, 1996; Pufahl and Fralick, 2004). Alternatively, Fe^{2+} could precipitate directly from the water column as iron silicates or green rust (Johnson et al., 2018; Tosca et al., 2015; Halevy et al., 2017). The true nature of this final step in massive iron formation deposition is difficult to ascertain due to diagenetic processing, metasomatism and metamorphism which transform primary iron formation mineralogy to iron-carbonates, iron-silicates, iron oxides and chert (e.g. Rasmussen et al., 2016; Robbins et al., 2019). Despite these uncertainties regarding the depositional and post-depositional record, it is agreed that a crucial requirement for iron formation deposition is the presence of low oxygen water masses, allowing high concentrations of dissolved ferrous iron Fe^{2+} to accumulate.

1.1 Models for Massive Iron Formation Deposition in Shelf Environments

Stratigraphically thick, massive iron formations have been classically tied to the global dynamics of broad, stable, continental shelf environments (Gross, 1983; Klein, 2005; Bekker et al., 2014). Within this framework, iron formation deposition on shelves has been interpreted as a dynamic of major transgressive events and not necessarily as a reflection of dramatic variations in ocean redox or ferrous iron concentrations (e.g. Ojakangas, 1983). These massive iron formation deposition models are consistent with extensive Archean deposits found in Australia and South Africa. There, the iron formation sedimentology, sequence stratigraphy, proximal platformal carbonate associations, and asymmetrical occurrence of iron formations across the platform margins support deep-water, sediment-starved facies interpretations (e.g. Klein and Beukes, 1992; Morris and Horwitz, 1983; Fischer and Knoll, 2009; Knoll and Beukes, 2009; Beukes, 1983). These deposits are predominantly banded iron formations (BIFs), interpreted to be chemical muds with well-developed, thin, primary laminations and bedding with alternating iron-rich and iron-poor layers, the iron poor-layers being dominantly chert (e.g. Fischer and Knoll, 2009; Simonson, 2003; Gross, 1983).

Although massive iron formations were deposited both before and after the GOE, they display sedimentological variations across this important atmospheric change. After the GOE, massive iron formations are predominantly deposited ca 1.88 Ga around Lake Superior (North America) as primarily granular iron formations (GIFs) rather than BIFs (Simonson, 2003; Bekker et al., 2014; Konhauser et al., 2017). GIFs are composed of "granule" clasts that range in size from fine to coarse sand and are well-rounded to angular (e.g., Van Hise and Leith, 1911;

Mengel, 1973; Simonson, 2003). However, these later ca. 1.88 Ga iron formations are also suggested to be shelf deposits because of 1) their size and extent (e.g. Kimberley, 1989), 2) the lack of evidence for subaerial exposures (e.g. Ojakangas, 1983; Simonson, 1984), 3) the lack of chemical and mineralogical variability expected from closed basins (e.g. Gole and Klein, 1981; Lepp, 1987), and 4) their conformable position within a transgressive sequence between subtidal quartzites and slope shales (e.g. Ojakangas, 1983; Simonson and Hassler, 1996). Problematically, recent work has demonstrated that the slope shales may be separated in time from iron formation deposition by at least 20 million years (Addison et al., 2005). Furthermore, documentation of cross stratification has been used by some authors to suggest that the granular iron formation may represent shallow-water deposits (~10s meters) (Simonson, 1985; Simonson, 2003), while alternatively, those bedding features may reflect deeper water storm deposits (Pufahl and Fralick, 2004). Therefore, it is still uncertain if all massive iron formations, and in particular the ca. 1.88 Ga massive iron formations, fit a transgressive systems tract, passive margin, shelf depositional model.

Furthermore, the driver of iron formation deposition is still unknown. If the passive margin shelf depositional model is correct, then the 1.88 Ga iron formation pulse may simply reflect a global transgression. Alternatively, iron formation deposition could be triggered by variation in the physical environment (e.g., a change in atmospheric oxygen, tectonic or magmatic events; Bekker, et al., 2014). Indeed, the ca. 1.88 Ga iron formation pulse has been attributed to changing atmospheric conditions, changing ocean oxygen and chemistry, extensive volcanism, and continental amalgamation and breakup dynamics (e.g. Rasmussen et al., 2012; Bekker et al., 2010; Ernst and Bell, 2010; Hamilton et al., 2009; Barley et al., 2005). Understanding both the depositional and tectonic framework is crucial for interpreting the global significance of the ca. 1.88 Ga iron formation pulse and distinguishing between these various models.

In order to address uncertainties in the depositional and tectonic context and key factors driving deposition of these post-GOE iron formation, we focus on ca. 1.88 Ga strata from the North American Gogebic range in the Lake Superior region (Fig. 1 a,b,c). Within the Lake Superior region, the Gogebic range in Michigan and Wisconsin was chosen as a target as previous work suggested that tectonic and volcanic activity accompanied iron formation deposition and a stratigraphic facies model has not yet been defined for the Gogebic range (Sims et al., 1984; Pufahl and Fralick, 2004; Cannon, 2008). If local volcanics are consistently found stratigraphically beneath the iron formation, this would provide compelling evidence for local volcanism as a trigger for the onset of iron formation deposition. To clarify local and regional relationships between tectonic and volcanic activity and iron formation deposition as well as test the passive shelf model for these ca 1.88 Ga iron formations, we make new stratigraphic observations and present updated mapping relationships of the Ironwood Iron Formation and the Emperor Volcanics. We combine our field observations with literature datasets to construct a sedimentologic and volcanic facies framework, identify variations in stratigraphy and elucidate the depositional context for the onset of iron formation. Our observations are then used to create a depositional and volcanic model that incorporates basin dynamics for the Gogebic region.

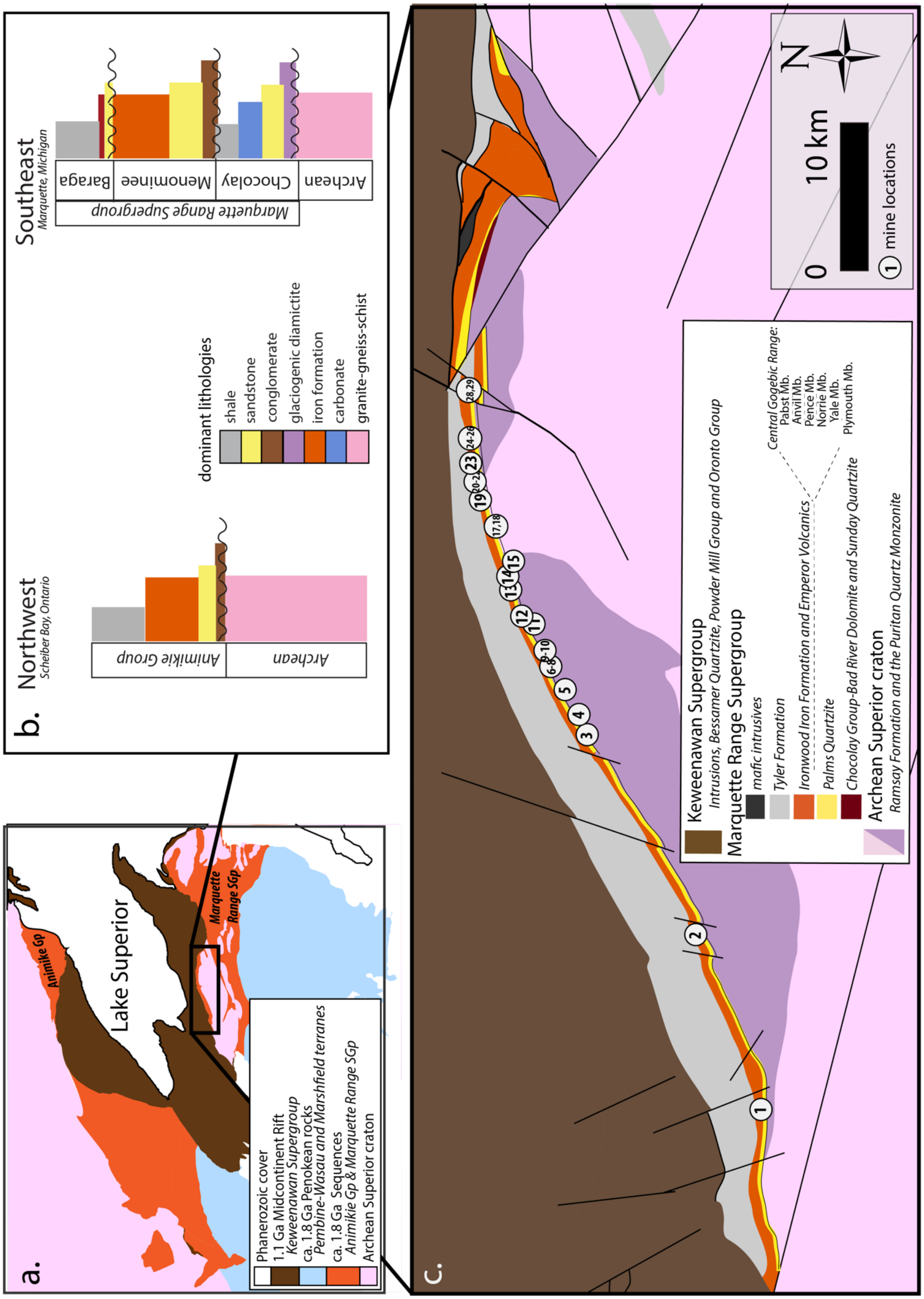

160 **Figure 1. Map. a.** Map depicting the sequences around Lake Superior (after Reed and Daniels, 1987; Sims, 1992; Schulz and Cannon, 2007). The Gogebic range is highlighted by the thick box. **b.** schematic stratigraphic sections. **c.** Inset of the Gogebic range. Numbers indicate mine locations of stratigraphic sections in figure 5.

1.2 Geologic overview

The iron formations around Lake Superior are part of the Paleoproterozoic Marquette Range Supergroup and Animikie Group that are separated by a major erosional unconformity from the Archean basement of the Superior craton (Fig. 1). The iron formation strata across the region are suggested to be correlative and deposited ca. 1.88 Ga. Specifically, in the Animike Group in Ontario, an age of 1,878.3 ± 1.3 Ma (TIMS Pb-Pb upper intercept of 5 zircon fraction; Fralick et al., 2002) has been obtained from a reworked ash layer in the upper Gunflint Iron Formation, while an ejecta layer correlated with the 1,850 Ma Sudbury impact event dates the stratigraphic top of iron formation in that area (Addison et al., 2005). Although the overlying greywacke-shale sequences (Tyler Formation in the study area and Virginia Formation in Minnesota) were initially thought to be in conformable contact with the iron formations, the identification of the Sudbury impact layer and an age of 1,832 ± 3 Ma (SHRIMP; 23 zircon analyses) from the overlying turbiditic units in Minnesota demonstrates an unconformity between the iron formation and overlying shale units (Addison et al., 2005).

In Michigan and Wisconsin, the entire Paleoproterozoic sequence experienced deformation related to the Penokean orogeny that culminated in the ca. 1.85 Ga collisions of the Pembine-Wasau and Marshfield terranes with the Superior craton margin (see Schulz and Cannon, 2007; Ojakangas et al. 2000; and references therein). After the Penokean orogeny, the region experienced erosion followed by the deposition and eruptions associated with the ca. 1.1 Ga Mesoproterozoic Midcontinent Rift system (e.g. Davis and Paces, 1990). About 30 million years after rifting, the Grenville orogeny to the east placed the region under compression, causing tilting and normal faults to be reactivated as reverse faults (Cannon, 1994).

The Gogebic range extends from Lake Gogebic in Michigan, westward ~128 km into Wisconsin (Fig. 1c). The region has been the focus of years of work (e.g. Van Hise and Lieth, 1911; Barret and Allen 1915; Hotchkiss, 1919; Laberge, 1963; Laybourn, 1979; Schmidt, 1980; Prinz 1981; Cannon et al., 2008). Archean rocks include the variably deformed and metamorphosed greenstones and granitoid rocks of the Ramsay Formation and the Puritan Quartz Monzonite (2,735 ± 16 Ma; 2 zircon fractions; Sims et al., 1985). These strata were metamorphosed up to amphibolite facies before being eroded and unconformably overlain by the Marquette Range Supergroup (MRS). Unconformably overlying basal siliciclastics and carbonates of the Chocolay Group is the Palms Quartzite that contains a transgressive sequence of basal muds, middle interbedded silt-sand-muds, and upper sands (Ojakangas, 1983). Current interpretations suggest that this Palms Quartzite transgressive sequence reflects deposition in tidal-subtidal conditions (e.g. Ojakangas, 1983).

Overlying the Palms Quartzite are the Ironwood Iron Formation and Emperor Volcanics. In the passive margin shelf depositional model, the Ironwood Iron Formation is a deeper water chemical sediment that is time-equivalent to the Palms Quartzite and represents a continuation of the transgression preserved in the Palms Quartzite (Ojakangas, 1983; Pufahl and Fralick, 2004). Based on mining data from the central part of the range, the Ironwood Iron Formation itself has been divided into five members: the Plymouth, Yale, Norrie, Pence, and Anvil members (e.g. Hotchkiss, 1919; Schmidt, 1980; Cannon, 2008). These Ironwood Iron Formation members have been difficult to distinguish on the eastern portion of the Gogebic range, in part due to the Emperor Volcanics near Wolf Mountain, Michigan (Trent, 1973; Dann 1978; Irving and Van Hise, 1982; Sims et al., 1990; Cannon, 2008). The Emperor Volcanics range from basaltic to dacitic compositions and have been metamorphosed to low greenschist facies. Variably overlying the Ironwood Iron Formation and Emperor Volcanics is the Tyler Formation. The final preserved strata in the region are the much younger Keweenawan Supergroup mixed siliciclastics and volcanics (Bessamer Quartzite, Powder Mill Group and Oronto Group).

2 Methods

2.1 Classification of iron facies

A facies table (Table 1) was constructed based on observations from outcrops and exposures surrounding Wolf Mountain combined with observations from Mount Whittlesey and published field and mine observations from along the Gogebic range (Hotchkiss, 1919; Schmidt, 1980; Laybourn, 1979; Cannon, 1984). In the Wolf Mountain locality, individual outcrops and test pits were found via field transects and published outcrop locations (Klasner et al., 1998 and Trent, 1973). At each outcrop, variations in textures, structures, bedforms, grain size and any contact relationships were recorded. Many researchers, especially in early works, utilized “cherty” vs “slaty”,"wavy" vs "parallel" terminology to describe Gogebic range Ironwood Iron Formation (Laberge, 1964; Dimroth, 1968; Dimroth and Chavel 1973). In this terminology “cherty” iron formation is typically composed of sand-sized chert and iron mineral grains within a chert matrix, and “slaty” iron formation is composed of laminated silt-sized chert and iron mineral grains. However, it has been suggested that the classification schemes that relied on “slaty” vs “cherty” terminology are not the most useful sedimentological classification (Simonson, 1985). Thus, we attempted to update classifications following the work of Simonson (1985) in utilizing the descriptive terminology of Pettijohn (1975) based on grain size and avoiding the use of terms which carry an implication of a particular chemical composition. Thus, we used terms such as rudite (grains >2mm), arenite (grains 0.0625-2 mm), and lutite (grains <0.063 mm). Furthermore, in much of the published literature on the Gogebic range Ironwood

Iron Formation, "wavy" terminology was used only to distinguish non-parallel bedding from parallel stratified beds (e.g. Hotchkiss, 1919). True wavy bedding displays laterally discontinuous ripples and marks the boundary between flaser and lenticular bedding (e.g. Reineck and Singh, 1980). Thus, we avoided this term unless referring to the specific depositional sedimentary structure. Finally, we chose to combine iron-carbonates, iron-oxides and iron-silicates under the classification of “iron minerals.” While there is important primary and diagenetic information in the distribution of iron minerals across the Gogebic Range, we made this decision to sidestep the debate regarding their original mineralogy (e.g. Rasmussen et al., 2016; Johnson et al., 2018; Robbins et al, 2019), and encompass the current mineralogical heterogeneity while maintaining focus on the stratigraphic and sedimentological details.

2.2 Classification of volcanic facies

Volcanics were described following standard terminology using descriptive terms and a facies approach (Cas and Wright, 1987; McPhie et al., 1993). Because of the diverse genetic processes involved in the formation of volcanic deposits, two descriptive categories were used, “volcaniclastic” or “coherent” (McPhie et al., 1993). The igneous term “volcaniclastic” is descriptive and applies to deposits composed predominately of volcanic particles (Fisher, 1961). The particles may be any shape or size and no specific clast forming processes, or settings are implied (autoclastic, pyroclastic, resedimented, and volcanogenetic sedimentary). The term “coherent” applies to deposits with distributed euhedral crystals that have narrow size ranges and lack volcanic particles. Coherent deposits occur principally from effusive lava flows and intrusions from cooling and solidification of molten lava/magma. In particular, the composition, textures, and flow and joint structures for coherent lavas and intrusions, and grainsize, component compositions and textures, and bedding structures for volcaniclastic deposits were recorded (Table 2). Then, facies associations were created in order to group volcanics into genetic classifications and likely eruptive phases.

2.3 Stratigraphic thicknesses across the Gogebic range

In the Wolf Mountain area from our refined geologic mapping, thicknesses were measured perpendicular to strikes and corrections for local dips were applied within each interpreted fault block. To obtain robust stratigraphic thicknesses across the Gogebic range, we compiled published mine sections and logs from the western Penokee gap to the eastern Mikado mine (see supplemental Table S1 for location information; (Hotchkiss, 1919; Laybourn, 1979; Schmidt, 1980). These sections were combined with our new stratigraphic section measurements and estimated thicknesses from our refined geologic mapping the Wolf Mountain area to construct a fence diagram along strike of the entire Gogebic Range.

3 Data and Interpretations

3.1 Facies descriptions

3.1.1 Facies descriptions of iron formation

In Wolf Mountain, there are iron formation outcrops in the north and central portions of the map area, along with scattered test pits (Fig. 2). To the west, partial sections are exposed, such as at Mount Whittlesey. As the most complete sections of the Gogebic range iron formations are located in now inaccessible mines and drill cores, reinterpreting the facies descriptions and interpretations without new first hand observations is problematic. In the supplemental text we have attempted to provide a reanalysis using the new facies framework but refer readers to Hotchkiss, (1919) and Schmidt (1980). The facies are briefly described here, and details are elaborated on in Table 1. Broadly the iron formation facies (Fig. 3a) fall into two categories, iron arenites (facies IF 1,2, 3) and iron lutites (facies IF 4, 5).

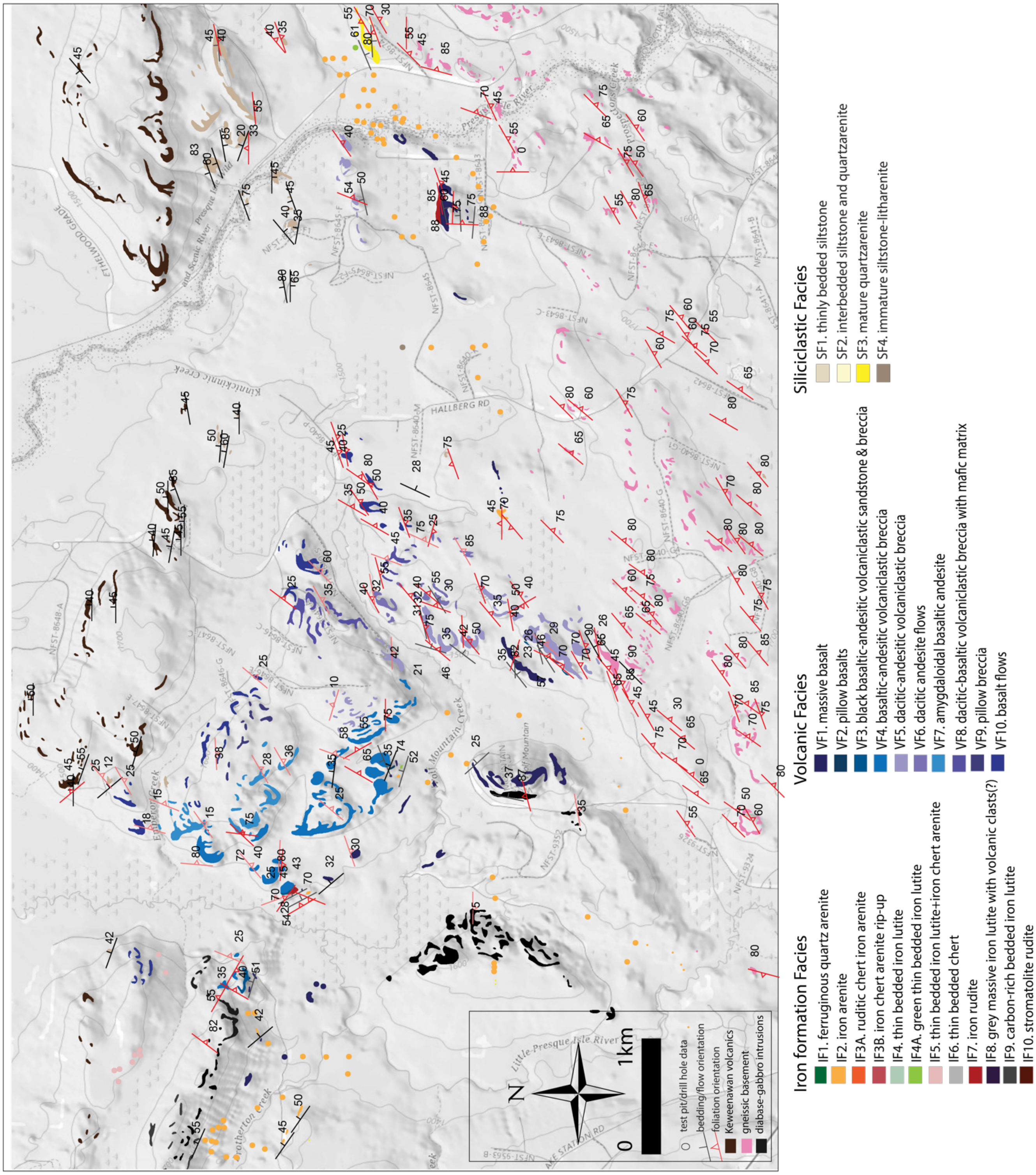

Figure 2. Outcrop map with new facies classifications. Also includes locations of test pits and old mine cores after Trent, 1973 and Klasner et al., 1998.

Facies IF1 is a ferruginous quartz arenite, with fine to medium quartz grains with some chert and lithic grains with chert cement. In the Wolf Mountain area it is the stratigraphically lowest exposure of the Ironwood Iron Formation and displays bi-directional and flaser crossbedding, fine iron lutite laminations and iron-mudstone partings (Fig. 3a). This facies is similar to units described elsewhere near the base of the Ironwood Iron Formation. Facies IF2 is an iron arenite (lacking quartz grains) and is moderately well sorted with medium to-coarse grained iron minerals or iron-coated chert grains intercalated with laminated and graded beds of gunflint grey-to brown colored medium-fine grained iron minerals (Fig. 3a). Additionally, it includes graded beds, slightly coarser massive, trough-crossbedded lenses, as well as minor amounts of rip-up intraclast fragments. This unit is likely similar to the "wavy cherty granular iron formation" (Hotchkiss, 1919) or "Upper cherty" previously described (Pufahl and Fralick, 2004). Facies IF2A is distinguished from IF2 by the greater abundance of thin laminated interbeds. Facies IF3 are similar to IF2 but includes interbeds dominated by angular fragments of green-grey chert and angular laminated chert and iron lutite clasts.

The facies IF4 and IF5 are dominated by iron lutites. IF4 is a thin bedded iron lutite. Facies IF4A is distinguished from IF4 by its striking greenish color. Across the Gogebic range, IF4 is similar to descriptions of the "parallel slaty iron formation" or "parallel laminated iron formation" (Hotchkiss, 1919; Pufahl and Fralick, 2004) and IF4A is similar to descriptions of the "footwall slate" by Hotchkiss (1919) and Schmidt (1980). Facies IF5 is similar to IF4, but it contains medium to very fine chert-iron arenite lenses along with pebble lenses. In the northwestern Wolf Mountain area, there are test pits displaying IF5. It is likely described previously as "parallel-wavy laminated lower slaty with minor ripple cherty units" (Pufahl and Fralick, 2004). Facies IF4 and IF5 were documented to have close association with the volcanics

(VF1 and VF4). In particular, outcrops of IF4 associated with both VF1 and VF4 were found to display syn-sedimentary faults (Fig. 3a). Microcrystalline bedded chert (facies IF6), were not identified in the map area but were found as clasts.

Two iron rudite facies were documented, a conglomeratic iron arenite of sub-rounded quartz cobbles in a tan-brown iron arenite matrix (IF7A), and a matrix-supported boulder conglomerate (IF7B). The latter was notable due to its large subrounded clasts, reaching boulder in size, supported by a fine-grained arenite matrix (Fig. 3a). The rounded clasts included bedded quartzite, and cherty iron formation (IF4), as well as angular, laminated, hematite-rich microcrystalline chert rip ups (IF 6) (Fig. 3a). Facies IF7 were documented to have close association with the volcanics (VF1).

Table 1. Sedimentary Facies Table

Facies Symbol. Name	**Description** Lithology/composition, grainsize, texture, structures/jointing/bedding	**Interpretation** Facies association, depositional environment, and formation-member occurrence
IF1. Ferruginous quartz arenite	Quartz arenite with iron-rich coating on grains and chert cement and fine chert lenses. Fine-medium grained rounded-well rounded quartz grains. Some lithic fragments. Well to moderately-well sorted grains coated with iron-rich coating (now hematite). <u>In the wolf mountain area:</u> a medium-coarse chert-quartz arenite with bi-directional and flaser crossbedding and fine iron lutite laminations.	Facies Assoc.: Underlies IF4 and IF10 tends to be at base Dep. Env.: Moderate to high energy, Intertidal, tidally influenced shoreline, Alternative: Shore-face transition zone with strong iron-lutite input Formations/members: Ironwood Iron formation undiff. and Plymouth member
IF2. Iron arenite	Moderately well sorted with medium-coarse iron-mineral and chert grains. Some chert grains are coated and display mudstone drapes and intraclasts (1–3 cm in length) of F4 or F6 at their bases. Can include massive, trough-crossbedded lenses that are slightly coarser. minor graded beds. Subunit IFN2A. Iron-Chert Arenite with iron-lutite interbeds. Moderately well sorted with medium-coarse iron-mineral and chert grains comprising lenses. Some chert grains are coated.	Facies Assoc.: Laterally equivalent to VF4, interbedded with VF3 Dep. Env.: Storm influenced Inner shelf (>10 ± 5m). Dominated by wave-storms causing linear sand ridges (water depths of 5-15m). Alternative 1: Surf and breaker zones below 0m, basal Upper-lower shoreface, Alternative 2: Intertidal subtidal sand shoal IF2A-Shelf transition from deep to storm influences. Alternative: Middle tidal flat Formations/members: Ironwood Iron formation undiff. and Plymouth, Norrie, Anvil mbs.
IF3. Iron-chert rudite-arenite	Subunit IF3A. Ruditic chert-iron arenite with lenses and layers of chert-arenite with interbedded lenses dominated by pebble clasts. Subunit IF3B. Iron-Chert Rip-up Rudite with angular fragments of green-grey chert and angular laminated clasts in a granular chert-iron matrix. Clast supported.	Facies Assoc.: IF3B-IF3A are gradational and associated with VF2 Dep. Env.: Gravely lag deposits on shelf, Alternative 1: Intertidal sedimentation on the foreshore or storm deposits. Alternative 2: IF3A-beach ridges Formations/members: Ironwood Iron formation undiff. and Plymouth, Norrie, Pence, Anvil mbs.
IF4. Thin bedded iron lutite	Uniform thin-bedded and parallel laminated iron formation comprised of fine well sorted iron-minerals (<0.1mm). Beds are laminated and cm-mm thick. Some interbedded thin microcrystalline chert beds (some internally graded). Subunit IF4A. Green thin-bedded iron lutite, very distinguishable green-greenish color. Subunit IF4B. Convolute bedded iron lutite-sometimes with interbeds composed entirely of iron lutite intraclasts	Facies Assoc.: Interbedded with IF2 and VF1, underlies VF4, laterally equivalent to IF6, IF2. Dep. Env.: Low energy Mid-outer Shelf, IF4B- Slumps formed during episodes of earthquake-induced subsidence or intertidal channel lag deposit, Alternative: Upper tidal flat Formations/members: Ironwood Iron formation undiff. and Plymouth, Yale, Pence, Anvil mbs.
IF5. Thin bedded iron lutite-chert arenite	Thin-bedded iron lutite comprised of very fine sand to silt iron-minerals. Interbedded with lenses and lag deposits 3-10 cm thick of medium to very fine chert- iron arenite. A few chert-arenite and pebble lenses. May contain chert interbeds.	†Facies Assoc.: laterally equivalent with IF9 and IF8 Dep. Env.: Mid Shelf, Alternative 1. Middle-upper tidal flat, Alternative 2. Shore-shelf transition Formations/members: Ironwood Iron formation-Yale Member, Emperor Volcanics-member A
IF6. Thin bedded chert	Thin-medium bedded (1-30cm beds) grey-greenish grey -yellow microcrystalline chert. Hematite staining can turn it red. Subunit IF6A. Thin bedded chert and lutite- dispersed interbeds of iron lutite or ferruginous siltstone Subunit IF6B. Thin bedded chert and iron arenite- interbedded chert-iron arenite lenses	†Facies Assoc.: Laterally equivalent to IF4 Dep. Env.: Shelf, Alternative IF6A: Intertidal/ lagoonal (6A), Alternative IF6B: Shoreface-foreshore Formations/members: Ironwood Iron formation-Plymouth, Pence mbs.
IF7. Iron rudite	Angular-rounded cobbles of laminated chert, iron lutite, and chert arenite. Highly variable and poorly sorted. Subunit IF7A. Conglomeratic iron arenite with sub-rounded to round quartz cobbles in a tan/brown iron arenite matrix. Beds are 20-30 cm and matrix supported. Subunit IF7B. Massively bedded lutite supported conglomerate with pebble -boulder subangular-subrounded clasts including bedded quartzite and laminated microcrystalline hematite-rich chert. Moderately-very poorly sorted clasts and matrix supported by brown-grey silt-fine sand sized matrix.	Facies Assoc.: IF7A underlies VF4. IF7B associated with VF1. Dep. Env.: Fault influenced deposition, Alternative 1: Backshore, Alternative 2: Debris flows Formations/members: Ironwood Iron formation undiff. and Pabst Member
IF8. Grey massive clastic unit	Dull grey massive beds. Some containing well-sorted black-grey rounded to angular fragments up to 4mm.	†Facies Assoc.: Laterally equivalent with IF5, IF9 Dep. Env.: Volcanically influenced sedimentation Formations/members: Ironwood Iron formation- Yale Member
IF9. Black laminated iron lutite	Dark grey-black partly pyritic, possibly argillaceous with no chert layers. Possibly volcanically influenced. Very finely laminated with disseminated black carbon.	†Facies Assoc.: Laterally equivalent with IF5 and IF8 Dep. Env.: Mid-outer Shelf, Alternative: Upper tidal flat Formations/members: Ironwood Iron formation-Yale Member
IF10. Stromatolite rudite	Stromatolites 2-10cm high (1-3cm in diameter). Stromatolites are white, grey or red, small and rather irregular and comprised of very fine laminae. Composed of chert with sparse hematite. Scattered quartz grains present as well as sub-rounded fine-medium chert/iron-mineral grains. Also included are oncoliths. Matrix is chert.	†Facies Assoc: Dep. Env.: Shelf reef buildups, Alternative: Intertidal foreshore beach Formations/members: Ironwood Iron formation-Plymouth Member
SF1. Shale	Well sorted Tan fine mudstone with parallel laminations.	Facies Assoc.: Unconformably overlying basement and gradationally underlying SF2. Dep. Env.: Low- energy supratidal -intertidal mud flats Formations/members: Palms Quartzite
SF2. Shale-siltstone-sandstone	Medium to well sorted mud-medium grains composing tan fine mudstone-sandstone. Displays flaser cross-beds and mudstone partings with sandstone lenses.	Facies Assoc.: Gradationally overlying SF1 and underlying SF2 Dep. Env.: Low-moderate energy intertidal mud flats Formations/members: Palms Quartzite
SF3. Mature sandstone	Sub rounded medium sized well-sorted Tan-beige mature sandstone. Parallel and cross bedded.	Facies Assoc.: Gradationally overlying SF2 Dep. Env.: Intertidal Moderate to high energy tidally influenced shoreline Formations/members: Palms Quartzite
SF4. Immature silt-sandstone	Chemically and texturally immature black-grey weathering poorly sorted siltstone-sandstone composed of Mud, quartz, lithics, plagioclase feldspar. Massively bedded. Graded beds described elsewhere (Cannon et al., 2008)	Facies Assoc.: Unconformably overlies VF9, VF10, IF5 and IF2 Dep. Env.: Slope-shelf turbidites Formations/members: Tyler Formation

†Specifically from stratigraphic descriptions by Hotchkiss, 1919; Schmidt, 1980; Pufahl and Fralick, 2004; and, in some cases, exposures at Mount Whittlesey

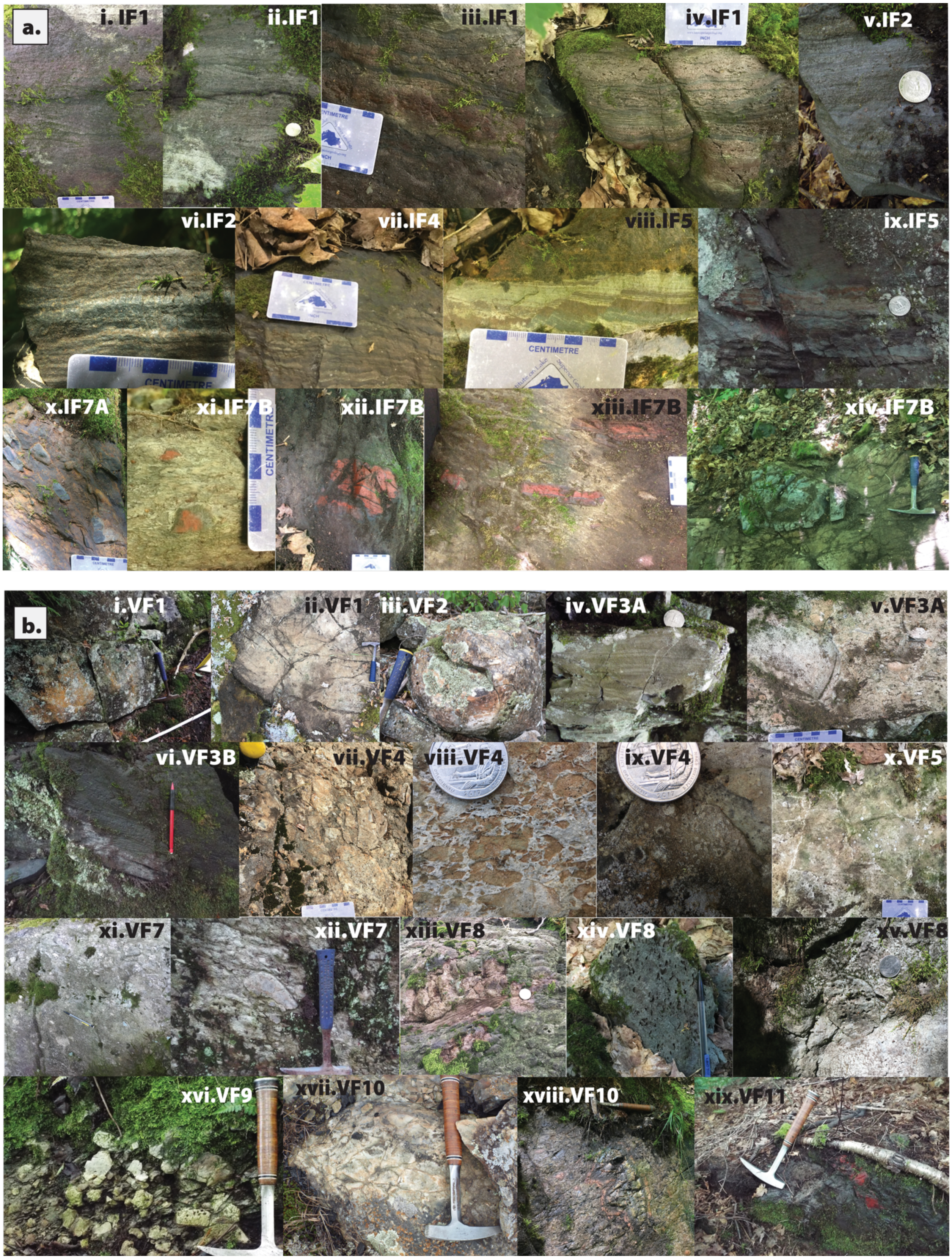

Figure 3. Field Facies Photos. **a.** Iron formation facies. **b.** Volcanic facies.

311

3.1.2 Facies descriptions of volcanics

Interbedded mafic, generally massive coherent basalt flows (facies VF1) are the stratigraphically oldest volcanics in the map area. These aphanitic flows with plagioclase phenocrysts weather pale brown and start to appear in resistant weathering knobs (0.5-25 m thick) in the recessive upper iron formation associated with facies IF4 and IF7 (Fig. 3b).

The other volcanics facies are generally more extensive and include both volcaniclastic and coherent facies, ranging in composition from mafic to felsic. Black basaltic-andesitic volcaniclastic breccia (VF3) is matrix supported and includes granule to cobble-sized clasts of orange-brown volcanic and altered glass fragments (Fig. 3b). This facies tends to weather orange to pale brown and the unit displays bedding structures (Fig. 3b). Facies VF3A is similar in composition but lacks large clasts and instead displays parallel laminations and cross bedding (Fig. 3b). Basaltic-andesitic volcaniclastic breccia (facies VF4) and volcaniclastic rocks ranging in composition from dacite to andesite (VF5) are the most extensive facies and are generally poorly sorted and massively bedded displaying features indicating subaqueous explosive eruptions such as curviplanar clasts, quenched margins and armored lapilli (Fig. 3b). Basal VF4 is associated with pillow basalts (VF2) and facies VF3 (Fig. 3b). The explosive VF4 are associated with fine-grained silty iron formation (IF5), that although not found in outcrop, are known from test pits and as well as old drill core data (Trent, 1973). VF4 transitions from basaltic-andesitic compositions to dacitic-andesitic compositions of VF5. At the base of VF5 a finer volcaniclastic unit is commonly found with an intermediate composition matrix and mafic sand to gravel-sized clasts. In certain localities, overlying and associated with the VF5 massive dacitic-andesitic volcaniclastic breccias are vesicular flows of similar composition (VF6) (Fig. 3b).

Overlying these explosive volcaniclastic facies are variable amygdaloidal basalt breccias (VF7) or a volcaniclastic facies with a mafic matrix and basaltic-dacitic clasts (VF8). The clast compositions of facies VF8 appear to grade from mafic-intermediate in the west and felsic to the east. Mafic clasts contain amygdaloidal fragments. Finally, facies VF9 and VF10 represent the stratigraphically youngest volcanics and are distinguished from the other mafic facies by their very dark green-black color combined with their dominantly coherent to autoclastic nature. Facies VF9 is a coherent-autoclastic basalt that includes pillow morphologies (Fig. 3b), while VF10 includes aphanitic basalts, with some amygdaloidal flows and jasper clasts (Fig. 3b).

3.2 Depositional Interpretations

3.2.1 Interpreted depositional environments of the Ironwood Iron Formation

The environmental interpretations were informed by existing work on iron formations (Ojakangas, 1983; Pufahl, 1996; Pufahl and Fralick, 2004; Edwards et al., 2012), as well as frameworks for shoreface and shallow siliciclastic marine facies (e.g. Reading and Reading, 1978; Reineck and Singh, 1980). However, interpreting the depositional environment is still difficult since deposition in recent settings hinges on biological indicators (e. g. Reading and Reading, 1978). By combining sedimentary structures and lithofacies associations with facies stacking patterns, contacts, and larger geometries, more discerning environmental interpretations can be made. Depositional environments were interpreted despite limitations imposed by incomplete exposure of outcrops and contacts.

Table 2. Volcanic Facies Table

Facies Symbol. Name	**Description** Lithology/composition, grainsize, texture, structures/jointing/bedding	**Interpretation** Facies association, depositional environment, and formation-member occurrence
VF1. Massive basalt	Coherent flows (30 cm – 3m thick) of tan-grey basalt. Generally non-vesicular and aphanitic although some contain plagioclase phenocrysts.	Facies Assoc.: IF4 and IF7 Dep. Env.: Subaqueous effusive eruptions and sheet flows (lack of pillows may indicate proximal environments). Formations/members: Emperor Volcanics, Ironwood Iron formation
VF2. Pillow basalt	Coherent, purple-brown colored basaltic andesite flows that weather brown. Pillows are generally aphanitic, do not have abundant vesicles, and display tortoise shell contraction cracks.	Facies Assoc.: Above IF4, IF5, IF7, below VF4 Dep. Env.: Subaqueous effusive eruptions Formations/members: Emperor Volcanics-member A
VF3. Black basaltic-andesitic volcaniclastic sandstone and breccia	General description: volcaniclastic basaltic andesite that is black when fresh. Subunit VF3A – Coarse poorly sorted volcaniclastic basaltic andesite weathers tan-beige. Cobble-to-sand-sized clasts consist of orange-brown crystal and volcanic lithic fragments and altered glass range in size. Certain clasts appear to be "pseudo fiame". Unit is generally matrix supported by fine grained matrix with plagioclase laths. Some units have parallel laminations or flow bands. Unit found only overlying the iron formation in the western portion of the map area. Subunit VF3B – Fine silt-sand basaltic-andesitic volcaniclastic sandstone (black in color when fresh and weathered, though iron-staining is prevalent) that is black fresh and black weathering with iron staining is more common. Unit is well sorted, parallel to cross-bedded, but with isolated sub-angular to sub-rounded jasper grains.	Facies Assoc.: Overlies-laterally equivalent to IF2 and underlies VF4 and VF5 Dep. Env.: Explosive mass flow deposit Formations/members: Emperor Volcanics-member A
VF4. Basaltic-andesitic volcaniclastic breccia	Volcaniclastic basaltic andesite that is green-purple color when fresh, and pale beige-brown when weathered. It is clast supported by cobble to sand-sized angular volcanic clasts in a matrix of the same composition, and generally poorly sorted and massively bedded. Clasts display pale-white margins, jig-saw fits, and curvi-planar surfaces. Well-sorted sand- sized lenses and beds occur throughout, some of these finer beds include armored lapilli.	Facies Assoc.: IF5 and overlies VF3B Dep. Env.: Explosive hyaloclastite deposit Formations/members: Emperor Volcanics-member A
VF5. Dacitic-andesitic volcaniclastic breccia	Volcaniclastic andesite that is pale green-grey when fresh, and weathers white-tan. This unit is clast supported by sand-cobble subangular-subrounded volcanic clasts in a matrix of the same composition. Some clasts are curviplanar and display quenched rims. The thick beds are poorly sorted and massive. Some beds appear to be reverse graded. A finer volcaniclastic unit with matrix of intermediate composition and sand to gravel clasts of mafic material commonly occurs at the base.	Facies Assoc.: overlies deposits of VF3-4, associated with VF6 and underlies VF7-VF8 Dep. Env.: Subaqueous hyaloclastite and epiclastite at base Formations/members: Emperor Volcanics-member B
VF6. Dacite-andesite flow	Coherent pale green-grey fresh andesite flows that weathers to a grey-pale tan color. Generally aphanitic with fine crystals of plagioclase and amphibole. Abundant vesicles aligned with flow banding and filled in with quartz and calcite. Rounded vesicular clasts are isolated, as well as discontinuous lenses of laminated units (VF5).	Facies Assoc.: Associated with VF5 (generally as fine lenses), tends to be more abundant up section Dep. Env.: No specific indicators, but given associations with VF5 likely subaqueous Formations/members: Emperor Volcanics-member B
VF7. Amygdaloidal basaltic breccia	Coherent purple-brown autoclastic basalt-breccia that weathers to a brown color. Aphanitic but contains abundant vesicles (now filled with quartz and calcite). The breccia is clast supported, and angular clasts are cobble sized with pale-white margins possess a jigsaw fit. Flows appear to be massive.	Facies Assoc.: Associated with VF8/overlying VF4/underlying VF9-VF10 Dep. Env.: Subaqueous hyaloclastite breccia Formations/members: Emperor Volcanics-member C
VF8. Dacitic-basaltic volcaniclastic breccia with mafic matrix	Volcaniclastic unit clast supported unit with cobble-pebble pale green-tan angular to subangular volcanic clasts in a mafic black-green matrix.	Facies Assoc.: Generally underlying VF9-10 and overlying VF5-6 Dep. Env.: Re-sedimented mass flow deposits Formations/members: Emperor Volcanics-member C
VF9. Pillow-breccia basalt	Coherent-autoclastic basalt. Black-green weathering and dark-grey fresh aphanitic basalts. Abundant epidote and qtz veins. Clast supported by cobble angular volcanic clasts displaying jigsaw fits and faint quenched rims. Some clasts display pillow morphologies.	Facies Assoc.: Associated with VF10 Dep. Env.: Subaqueous hyaloclastite-pillow breccia Formations/members: Emperor Volcanics-member D
VF10. Dark basalt flow	Coherent-autoclastic dark black-green, aphanitic basalt. Some units are amygdaloidal and contain jasper clasts.	Facies Assoc.: Associated with VF9 and overlies IF5 Dep. Env.: No specific indicators, but given lateral associations with VF9 likely subaqueous Formations/members: Emperor Volcanics-member D

354

The Gogebic range generally has been interpreted as displaying two transgressive-regressive upwards sequences involving the transitions from dominantly iron arenites, to iron lutites, and back to iron arenites. The currently accepted model for a facies progression from IF4 to IF2 is a regressive deep shelf-to shallow shelf storm deposit sequence. This is based on past work at Mount Whittlesey that highlighted coarsening upward, gradational relationships from iron-chert lutites to arenites and interpreted both to be shelf deposits, with the coarser units reflecting storm deposits, and the sequence reflects progradation of offshore directed storm currents (Pufahl and Fralick, 2004). This model draws on comparisons to modern shelf sand deposits associated with autochthonous shell layers at the base of a storm sand layer (e.g. Reineck and Singh, 1980). However, modern continental shelf deposits are alternatively suggested to be reworked relict sands from Holocene and Pliocene low stands, and thus may not be a proper analog for these iron arenite deposits (e.g. Reineck and Singh, 1980).

A further complication is that not all iron arenite facies require the same depositional environment. For example, facies IF2 could be shelf storm deposits as previously suggested, or alternatively shoreface sands. Flaser and lenticular bedding are observed within facies IF1 and IF2, yet flaser-lenticular bedding is not uniquely indicative of a specific environment or water depth, as flaser, lenticular and sand-clay alternating bedding are commonly observed in sub-tidal, intertidal, lagoonal, fluviatile and deltaic environments as well as coastal sand and shelf transition zone environments (Reineck and Wunderlich, 1968; Terwindt, 1971; Reineck and Singh, 1980). Furthermore, the laminated iron-lutites could be deep-water shelf deposits or tidal mudflats. Although these two environments can be distinguished by mudcracks forming on tidal mudflats, those are ubiquitous only in arid conditions with high tidal ranges (Reading and Reading, 1978). We suggest that the current available evidence does not unequivocally support a particular depositional environment for the Ironwood Iron Formation. Although the coarsening upward sequence is consistent with a shelf to shoreface regressive sequence, a mudflat to subtidal transgressive sequence could also be permissible.

3.2.2 Interpreted Emperor Volcanics Eruptive Sequence

The massive basalt flows (VF1) associated with the upper iron formation are included in the Ironwood Iron Formation, not the Emperor Volcanics. This facies is not found to directly underlie iron formation facies, but instead occurs near the upper contact between the often covered and recessive iron formation and the resistant outcrops of the explosive eruptions marking the onset of the Emperor Volcanics (Fig. 4). The main volcanic phases were grouped into Emperor Volcanics members A, B, C and D (Fig. 4a). First, features of member A (including facies VF2-VF4), namely pillow basalts, hyaloclastites and armored lapilli are consistent with subaqueous eruptions. Although accretionary lapilli develop in air fall eruptions, armored lapilli can form with wet ash around a solid nucleus during hydrovolcanic eruptions (Cas and Wright, 1987). Additionally, fine-grained mafic volcaniclastic units can originate in subaqueous hyaloclastite density currents (e.g. Cas and Wright, 1987). Important for questions regarding the relationship between volcanism and iron formation, are the mapped locations of IF5, V3 and V4. Iron formation facies IF5 are found in test pits in the northwestern portion of the map area (Figure 3). Although not extensive in outcrop, due to the geometry of their locations, it is likely that these test pits represent in-situ lithologies. These iron formation localities appear to overlie early eruptive facies VF3 and are laterally equivalent to VF4. These eruptive and depositional relationships suggest that the Emperor Volcanics member A eruptions are likely coeval and time-equivalent with iron formation deposition. Member B is marked by evolved intermediate to felsic compositions (facies VF5-VF6), but a similar eruptive environment to member A. The mixed volcaniclastics of member C (facies VF8) contain clasts of members A and B, and thus represent re-deposition of members A and B within a mafic matrix. Synchronously, there is evidence for mafic volcanic autoclastic breccia being deposited as amygdaloidal flows with jigsaw fitted brecciation (facies VF7). Member C could represent reduced subaerial or subaqueous eruptions accompanied by re-mobilization of previously erupted volcanics. Finally, member D (facies VF9 and VF10) is characterized by effusive basalt flows with hematite-stained chert clasts. It could represent slightly younger volcanism, as it overlies members A-C as well as iron formation facies IF5. As member D basalts include pillow fragments and quenched features, they also represent subaqueous eruptions.

3.3 Structural interpretations

The location and orientation of major faults are identified based on thickness variations between basal contacts, as well as with measured orientations of smaller, outcrop-scale, syn-sedimentary faults observed in the field. The onsets of certain eruptive facies were interpreted as marker horizons. In particular, we used (1) the onset of the explosive basaltic andesite hyaloclastites (member A), (2) the onset of dacite-andesite hyaloclastites (member B), and (3) the onset of effusive dark basalt flows and pillows (member D). These marker horizons allowed the geometry of fault blocks in the map area to be refined and major new named faults to be identified (Fig. 4a). This detailed approach has allowed new and different interpretations of regional faulting and dynamics to be clarified (Fig. 4b,c,d).

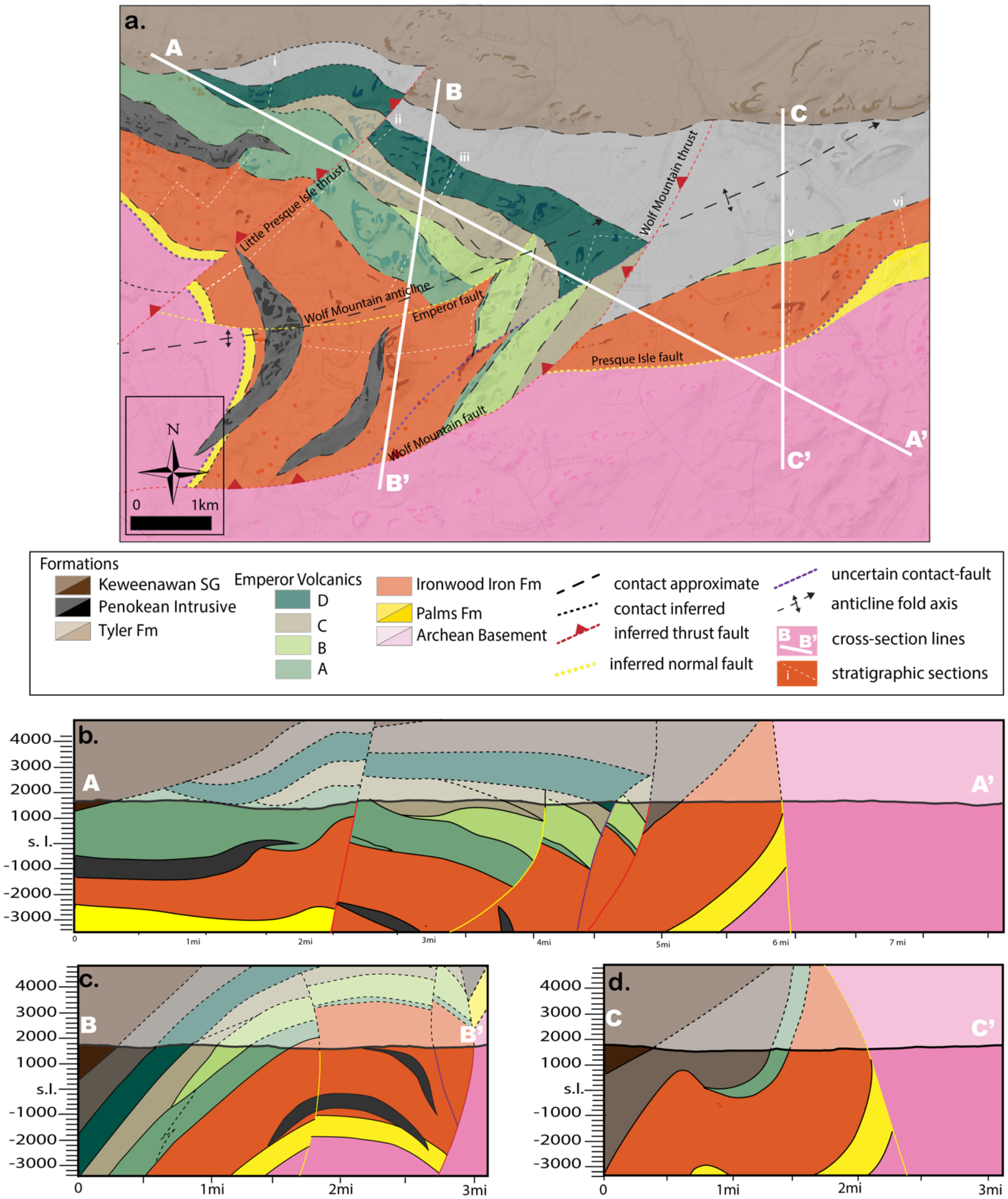

Figure 4. a. Wolf Mountain area map interpretations with depositional and faulted contacts. The locations of cross-sections and sections used in fence diagram are indicated (i, ii, iii, iv). **b, c, d**. Wolf Mountain map cross sections.

To highlight these interpretations, each mapping relation is considered in turn (Fig. 4), starting with the younger deformation (post Keweenawan thrusts and Penokean compressional structures), and then considering the Paleoproterozoic structures and deformation which are particularly important for our interpretations. There are three important Keweenawan/Penokean structures, these are the Little Presque Isle thrust, and the Wolf Mountain Anticline and thrust fault. Thrust faulting along the Little Presque Isle thrust was identified based on displacement of the Keweenawan basal contact with the Tyler Formation (Fig. 4). This fault activity is likely due to Grenville-aged reverse faulting (e.g. Cannon et al., 2008; Cannon, 1990). The Wolf Mountain Anticline, plunging to the northeast in its present-day geometry and impacting all the Paleoproterozoic strata, is the most obvious structural feature in the area. Although not previously recognized, we observed displacements in the basal Tyler Formation-Emperor Volcanics contact, suggesting the existence of an associated Wolf Mountain thrust. This newly identified structure explains both stratigraphic differences across its east and west sides, as well as the associated generation of the Wolf Mountain Anticline.

With this more recent deformation accounted for, there are three earlier Paleoproterozoic structures with potential importance, the Emperor fault, Wolf Mountain fault, and Presque Isle fault. The mapped locations of the onset of explosive activity (Emperor Volcanics member A) and the associated underlying iron formation thickness variations were used to reveal and infer fault locations. Specifically, by tracing the location and identifying possible offsets in the basal iron formation contact, as well as its contact with the explosive activity of Emperor Volcanics member A, the presence of syn-eruptive and syn-depositional faults were highlighted.

It was previously suggested that the Emperor Volcanics erupted into an extensional graben between the Little Presque Isle thrust and Presque Isle fault, as the volcanics appear thicker to the east of the Little Presque Isle thrust (Cannon et al., 2008). Yet, when the map relationships and stratigraphy are restored prior to intrusions and Keweenawan faulting, dramatic thickness variations or displacements of the initial explosive volcanism (member A) do not exist. There may have been some extension, but because of this dearth of dramatic thickness variations and displacements across it, we argue that the Little Presque Isle thrust was not a crucial syn-eruptive fault. Instead, we propose a new fault, we have named the Emperor fault, that is associated with the initial eruptive phases of the Emperor Volcanics. The Emperor Fault is highlighted by displacements of the basal member A contact south-east on the north side. As the basal member D contact is not dramatically displaced, faulting may have ceased by the later eruptions. The iron formation thickness variations that existed prior to the explosive eruptions of the Emperor Volcanics suggest that the Wolf Mountain thrust may have reactivated an original normal fault, we have named the Wolf Mountain fault. Finally, we followed the existing framework regarding the basement-Paleoproterozoic strata contact as the syn-depositional Presque Ilse fault (e.g. Cannon et al., 2008).

In our new framework, the Emperor fault and Wolf Mountain fault are syn-depositional, syn-eruptive listric faults related to extensional faulting along the main Presque Ilse fault. This contrasts with previous authors (e.g. Prinz, 1967) who explained the extreme iron formation thickness changes as being due to later faults striking parallel to bedding. Those interpreted structures were proposed to have been folded by the Wolf Mountain anticline (Klasner et al., 1998; Cannon et al., 2008). However, in the study location there is no direct evidence for those later bedding parallel faults or repetition. Although large scale faults are not exposed, the direct observations of potential fault scarp conglomerates and small scale syn-depositional faults along with inferred thickness changes, lead us to suggest that there is true stratigraphic thickening in the area related to fault activity.

4 Discussion of Results

4.1 Gogebic range stratigraphic variations

Based on our facies-focused mapping in the Wolf Mountain area combined with a new compilation of previous stratigraphic data from pits and mines, we find significant stratigraphic variations within the Ironwood Iron Formation (Fig. 5; Fig. 1c for reference on member stratigraphy and supporting information for more details). By incorporating stratigraphic data along the rest of the Gogebic range, about 200 m of stratigraphic thickness increase is seen approaching the easternmost Gogebic range. Most of this is manifest midway through the stratigraphy in units dominated by facies IF4, IF5, IF8 and IF9 (Yale Member) and above, although the basal stromatolite rudite (IF10) facies within the Plymouth Member is particularly thick in the eastern Eureka and Mikado Mines. Within the Yale Member, mixed thin bedded iron lutite to iron and chert arenite (IF5) facies approaches 113 meters in thickness in the Mikado mine. This thickening is accompanied by the appearance of facies IF8, a potentially distal equivalent of the Emperor Volcanics (Schmidt, 1980). Further up section, thickness variations within stratigraphic sections correlate with the appearance of coarser facies IF2, IF3 (Anvil Member). The thickness of the uppermost iron arenite facies IF2 (Anvil Member) increases abruptly from the Windsor Mine to the Ashland mine, and continues to increase substantially eastward towards the Eureka Mine. These thickness variations are clearly seen across the Gogebic range stratigraphic fence diagram plotted with the IF8, IF9 and the explosive hyaloclastites (VF4 and VF5) as datums (Fig. 5). These thickness variations include results from our high-resolution facies mapping in the Wolf Mountain area.

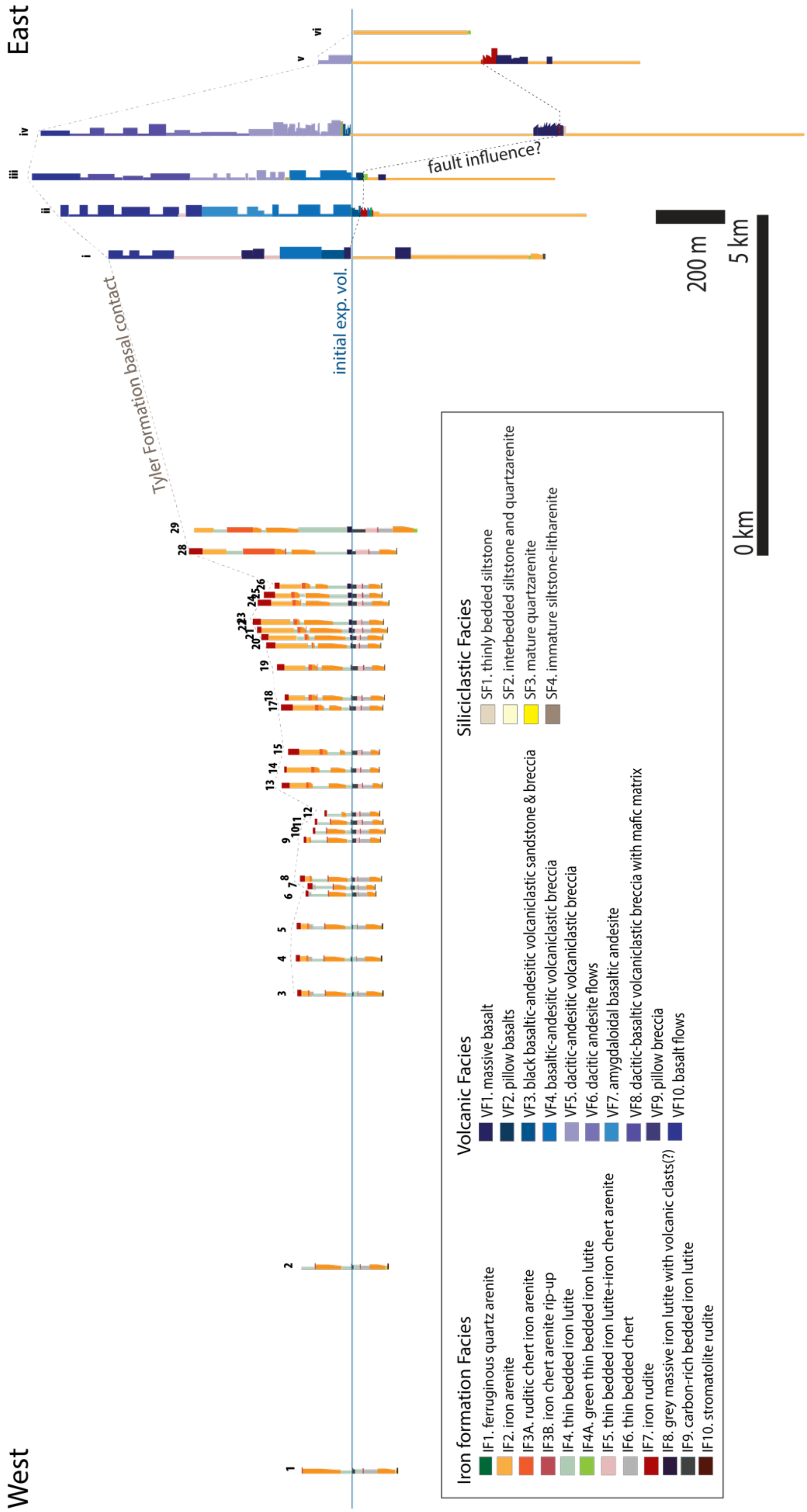

Figure 5. Stratigraphic fence diagram for the Gogebic range. Numbers correspond to sections and mine data (see fig. 1 and SI) and roman numerals indicate sections in the Wolf mountain area, see fig. 4.

Analysis of this compilation and associated fence diagram, suggests that thickness variations start at or below the base of the Yale Member. This is consistent with some of the suggestions by Hotchkiss (1919) and Schmidt (1980). Furthermore, we posit that the thickness variations reflect fault-influenced sedimentation in the Gogebic basin by the time of Yale Member deposition. This earlier onset of active sedimentation explains why Schmidt (1980) had such difficulty in matching his general Yale Member observations (mostly from the central-eastern part of the Gogebic range) with the Yale Member details from Hotchkiss (1919) which was primarily based on work in the western Gogebic range.

4.2 Gogebic range basin dynamics

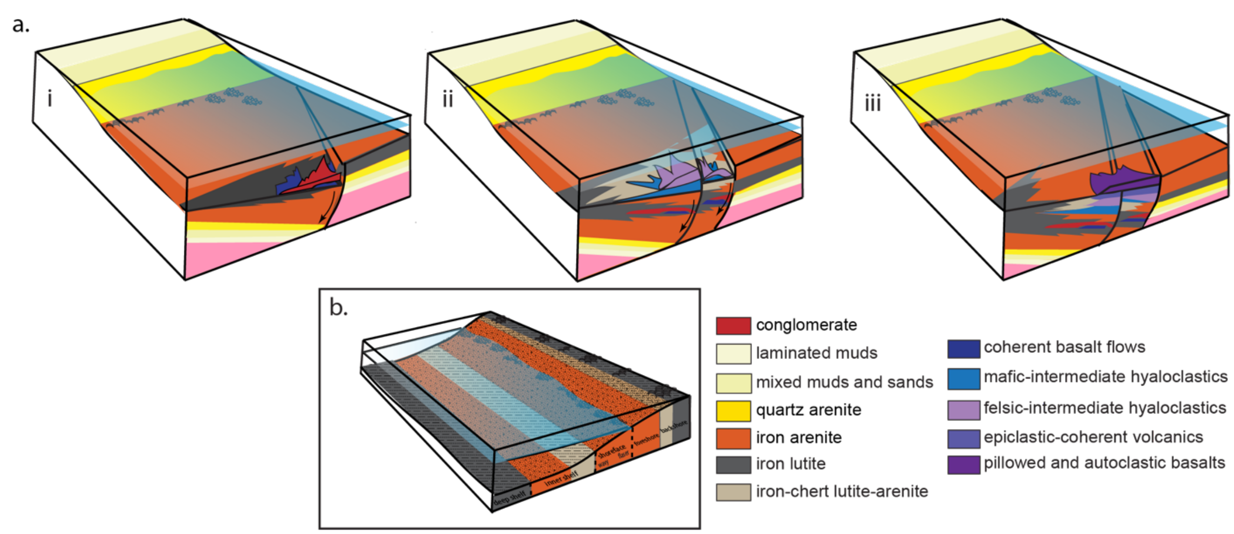

Figure 6. Model of Basin dynamics. a. steps in Gogebic basin development: i. iron formation deposition followed by onset of effusive volcanism and faulting. ii. Start of explosive hyaloclastite eruptions and continued faulting and iron formation deposition. iii. Return to effusive volcanism that may or may not postdate faulting and iron formation deposition**. b.** Although the model in figure 6a utilizes a model following Ojakangas (1983) model with iron formation deposition constrained to the shelf, here is depicted an alternative model with iron formation deposited at shallow depths.

The basin dynamics are highlighted through the identified facies relationships within the Emperor Volcanics in the Wolf Mountain locality. The location and orientation of major syn-sedimentary faults were identified based on thickness variations of the iron formation underlying the explosive volcanic facies across the map area, as well as with measured orientations of smaller, outcrop-scale, syn-sedimentary faults observed in the field. Based on our results, we propose the following model for Gogebic range basin dynamics during iron formation deposition (Fig. 6). After iron formation deposition commenced, the eastern Gogebic range started experiencing faulting and effusive basaltic magmatism (Fig. 6ai). This faulting continued, while the magmatism changed from mafic to intermediate, explosive hyaloclastites, followed by intermediate–to-felsic hyaloclastites (Fig. 6aii). During faulting and explosive subaqueous eruptions, iron formation deposition continued across the Gogebic range with significant lateral facies variability, as evidenced by coarse fault-scarp conglomerates, and juxtapositions of iron lutite and iron arenite dominated units. Subsequently, there was a change in volcanism to effusive amygdaloidal flows accompanied by remobilization and reworking of the previously-erupted volcanics. Finally, sedimentation via re-mobilization was followed by a return to effusive basaltic magmatism that could have postdated the iron formation deposition and faulting in the area (Fig. 6aiii). Broadly, given this integrated stratigraphic dataset, variations in sedimentology, facies and stratigraphy suggest that much of the Gogebic range iron formation was deposited in an active extensional tectonic setting.

4.3 Implications for models of passive margin, shelf sedimentation of massive iron formation deposits

Given this integrated stratigraphic dataset from across the Gogebic range, we suggest that not all massive iron formation deposits are passive margin shelf deposits. Although the sedimentological data presented here do not distinguish between shelf and shallower water environments, we document and highlight stratigraphic thickening linked to facies changes in coarse conglomerates and inferred syn-sedimentary faults. We interpret these thickness variations to be tectonically mediated and suggest that the Ironwood Iron Formation may not be consistent with passive-margin deposition. This conclusion, while at odds with the transgressive model (Ojakangas, 1983), is supported by various tectonic frameworks that the iron formations of the Superior region were deposited in an active basin such as a foredeep basin (Hoffman, 1987), an extensional back-arc basin (Fralick et al., 2002), or in rift basins formed from transpressional docking of an oceanic arc (Schneider et al., 2002). Here, evidence is presented, independent of an external tectonic framework, that supports the conclusion that not all massive iron formations are passive margin shelf deposits.

4.4 The trigger for iron formation deposition: transgression or something more?

In the transgressive model for iron formation proposed by Ojakangas (1983), iron formation is not deposited in shallow waters as the surface water mass is too oxic to allow ferrous iron to accumulate in high enough concentrations. Iron formation deposits are found at the chemocline between oxic surface waters and basinal ferruginous waters (Simonson and Hassler, 1996), as well in deeper waters on shelves during storms due to the mixing of oxic water with ferruginous water masses (Pufahl and Fralick, 2004). The implication of the transgressive model is that iron formation deposition results from global transgressions and occurs on and within shallow continental passive-margins. If the passive-margin framework is not accurate, an external trigger for punctuated iron formation deposition is possible via any number of mechanisms, such as (1) lowered global atmospheric O_2 shifting the chemocline, (2) aqueous O_2 levels shifting the chemocline, (3) tectonic activity leading to restricted basins, or (4) intense local volcanism and increased hydrothermal Fe^{2+} input (e.g. Isley and Abbott, 1999; Bekker et al., 2014).

Stratigraphic relationships and datasets presented here illustrate the dynamic nature of the Gogebic basin. Rather than the simple transgressive passive-margin model for iron formation deposition, an external trigger for iron formation deposition may need to be invoked. However, as the field relationships suggest that volcanism occurred after iron formation deposition started, a local volcanic trigger for the Ironwood Iron Formation should not be considered. Instead, if volcanism is indeed important for initiating iron formation deposition in this instance, it could be in the form of distal volcanism such as a regional change in the tectonic regime, a subaqueous plume event or enhanced mid-ocean ridge spreading. Finally, given the coarse-grained iron formation facies with a range of current-generated sedimentary structures, we highlight the possibility of an alternative shallow water iron formation depositional model, where iron formation was deposited in both deep and shallow environments (Fig. 6b). However, this model needs to be constrained by and tested with additional observations particularly focusing on the transition from the siliciclastic Palms Quartzite and the Ironwood Iron Formation, the focus of our ongoing work.

5 Conclusions

Here we have combined new stratigraphic and mapping relationships with mine data and logs to refine the basin model for the Ironwood Iron Formation deposition and Emperor Volcanics eruption. Our new Wolf Mountain thrust explains the development of the Penokean Wolf Mountain anticline. Identification of the new Emperor fault provides a framework to understand stratigraphic thickening. Importantly, bedding parallel faults are not necessary to explain the thickness changes at Wolf Mountain, and the thickness increase is part of a general thickening trend across the Gogebic range tied to syn-sedimentary faulting within the basin and also highlighted by sedimentological expressions of syn-sedimentary faulting. Thus, the Gogebic range Ironwood Iron Formation deposition is not consistent with a passive margin. This point is significant as it requires an external trigger for the onset of iron formation deposition. Although not the first to discuss the possibility of a tectonically active dynamic environment, we are the first to present datasets to quantify and explain the westward thickening in support of tectonic activity (not a passive margin) during iron formation deposition. This fault-influenced iron formation depositional model may not hold for all the post-GOE iron formation basins, but the possibility should be explored.

Finally, our datasets also suggest that the initiation of significant local volcanism does not coincide with onset of Ironwood Iron Formation deposition. Thus, intense local volcanism cannot be invoked as a trigger for iron formation deposition. Furthermore, as the onset of faulting may have post-dated the onset of iron formation, it is not clear if a particular regional tectonic setting triggered the iron formation pulse. Although the onset might have been coincident with global oceanic perturbations, the equally permissible shallow water depositional environments could imply that iron formation deposition was triggered by chemocline shallowing due to decreased atmospheric oxygen. Other potential global mechanisms impacting the pH might be possible if the original Ironwood Iron Formation minerals were not ferri-oxyhydroxides. Whatever the cause for the onset, the Ironwood Iron Formation basin is not consistent with a passive-margin, and this work highlights the importance of combined sedimentological facies and stratigraphic approaches in reevaluating depositional models for post-GOE iron formations.

Acknowledgments, Samples, and Data

A. Eyster would like to thank Julia Wilcots for assistance in the field. We thank the Bergmann group for their support and comments on early drafts of the manuscript, and C. Condit and D. Ojakangas for helpful discussions. Data used in figures and analysis can be found in the supporting information and https://doi.org/10.5061/dryad.1g1jwsts1. Per Dryad rules, the dataset will remain private until the manuscript has been accepted. For private access during the review period use: https://datadryad.org/stash/share/ZPQoZPK39RWYNrP2lAt55tPEcbiVwAiEyb4o6FHSIHI Financial support for this research was provided by the MIT EAPS W.O. Crosby Postdoctoral Fellowship to A. Eyster and the Packard Foundation to K. Bergmann. There are no real or perceived financial conflicts of interests for any of the authors.

References

Aldrich, H.R., 1929. The geology of the Gogebic iron range of Wisconsin: Wisc. Geol. Nat. Hist. Survey, Econ. ser., Bull.

Allen, R.C. and Barrett, L.P., 1915. A revision of the sequence and structure of the pre-Keweenawan formations of the eastern Gogebic iron range. Michigan Geological and Biological Survey Publication, 18, pp.33-83.

Bekker, A., Planavsky, N., Rasmussen, B., Krapez, B., Hofmann, A., Slack, J., Rouxel, O. and Konhauser, K., 2014. Iron formations: Their origins and implications for ancient seawater chemistry. In Treatise on geochemistry (Vol. 12, pp. 561-628). Elsevier.

Beukes, N.J., 1983. Palaeoenvironmental setting of iron-formations in the depositional basin of the Transvaal Supergroup, South Africa. In Developments in Precambrian Geology (Vol. 6, pp. 131-198). Elsevier.

Cannon, W.F., 1973. The Penokean orogeny in northern Michigan. Huronian stratigraphy and sedimentation: Geological Association of Canada Special Paper, 12, pp.251-271.

Cannon, W.F., 1984. The Gogebic Iron Range: a sample of the northern margin of the Penokean fold and thrust belt (No. 1730). US Department of Interior, US Geological Survey.

Cannon, W.F., 1994. Closing of the Midcontinent rift-A far—field effect of Grenvillian compression. Geology, 22(2), pp.155-158.

Cannon, W.F., Schulz, K.J., Horton, J.W. and Kring, D.A., 2010. The Sudbury impact layer in the Paleoproterozoic iron ranges of northern Michigan, USA. GSA Bulletin, 122(1-2), pp.50-75.

Cas, R.A.F. and Wright, J.V. (1987) Volcanic Successions: Modern and Ancient. Allen and Unwin, London.

Davis, D.W. and Paces, J.B., 1990. Time resolution of geologic events on the Keweenaw Peninsula and implications for development of the Midcontinent Rift system. Earth and Planetary Science Letters, 97(1-2), pp.54-64.

Edwards, C.T., Pufahl, P.K., Hiatt, E.E. and Kyser, T.K., 2012. Paleoenvironmental and taphonomic controls on the occurrence of Paleoproterozoic microbial communities in the 1.88 Ga Ferriman Group, Labrador Trough, Canada. Precambrian Research, 212, pp.91-106.

Eugster, H. P., and Chou, I.-M., 1973, Depositional environments of Precambrian banded iron-formations: Economic Geology, v. 68, p. 1144-1168.

Fisher, R.V. 1961. Proposed classification of volcaniclastic sediments and rocks. Geological Society of America Bulletin 72: 1409-1414.

Fralick, P., Davis, D.W. and Kissin, S.A., 2002. The age of the Gunflint Formation, Ontario, Canada: single zircon U-Pb age determinations from reworked volcanic ash. Canadian Journal of Earth Sciences, 39(7), pp.1085-1091.

Govett, G.J.S., 1966, Origin of banded iron-formations: Geological Society of America Bulletin, v. 7, p. 1191-1212.

Hoffman, P.F., 1987. Early Proterozoic foredeeps, foredeep magmatism, and Superior-type iron-formations of the Canadian Shield. Proterozoic Lithospheric Evolution, 17, pp.85-98.

Hotchkiss, 1919. Geology of the Gogebic range and its relation to recent mining developments: engineering and mining Journal, v. 108, p. 443-452, 501-507, 537-541, 577-582.

Isley, A.E. and Abbott, D.H., 1999. Plume-related mafic volcanism and the deposition of banded iron formation. Journal of Geophysical Research: Solid Earth, 104(B7), pp.15461-15477.

Johnson, J.E., Muhling, J.R., Cosmidis, J., Rasmussen, B. and Templeton, A.S., 2018. Low-Fe (III) Greenalite Was a Primary Mineral from Neoarchean Oceans. Geophysical Research Letters, 45(7), pp.3182-3192.

Johnson, J. E., & Molnar, P. H. 2019. Widespread and persistent deposition of iron formations for two billion years. Geophysical Research Letters, 46. https://doi.org/10.1029/2019GL081970

Klasner,J.S., LaBerge, G.I,. and Cannon, W.F. 1998. Geologic map of the Eastern Gogebic iron range, Gogebic County, Michigan. I-2606. USGS.

Klein, C., and Beukes, N.J., 1992, Time distribution, stratigraphy, and sedimentologic setting, and geochemistry of Precambrian iron-formations, in Schopf, J.W., and Klein, C., eds., The Proterozoic Biosphere: A Multidisciplinary Study: Cambridge, UK, Cambridge University Press, p. 139–147.

Knoll, A.H. and Beukes, N.J., 2009. Introduction: Initial investigations of a Neoarchean shelf margin-basin transition (Transvaal Supergroup, South Africa). Precambrian Research, 169(1-4), pp.1-14.

LaBerge, G.L., 1973. Possible biological origin of Precambrian iron-formations. Economic Geology, 68(7), pp.1098-1109.

Laybourn, D. P. 1979. The Geology and Metamorphism of the Ironwood Iron-formation, Gogebic range, Wisconsin. PhD. Thesis. University of Minnesota. ,p. 446.

Laybourn, D.P., 1979. The Geology and Metamorphism of the Ironwood Iron-formation, Gogebic range, Wisconsin (Doctoral dissertation, University of Minnesota).

McPhie J, Doyle M, Allen R. Volcanic Textures: A Guide to the Interpretation of Textures in Volcanic Rocks. Centre for Ore Deposit and Exploration Studies, University of Tasmania, c1993.; 1993

Morris, R.C. and Horwitz, R.C., 1983. The origin of the iron-formation-rich Hamersley Group of Western Australia—deposition on a platform. Precambrian Research, 21(3-4), pp.273-297.

Ojakangas, R.W., 1983. Tidal deposits in the early Proterozoic basin of the Lake Superior region—The Early Proterozoic geology of the Great Lakes region, 160, p.49

Ojakangas, R.W., Morey, G.B., Southwick, D.L., 2001. Paleoproterozoic basin development and sedimentation in the Lake Superior region, North America. Sediment. Geol. 141–142, 319–341.

Pettijohn F. J. (1975), Sedimentary Rocks, Harper & Row, ISBN 0-06-045191-2

Pietrzak-Renaud, N. and Davis, D., 2014. U–Pb geochronology of baddeleyite from the Belleview metadiabase: Age and geotectonic implications for the Negaunee Iron Formation, Michigan. Precambrian Research, 250, pp.1-5.

Prinz, W.C., 1981. Geologic Map of the Gogebic range-Watersmeet Area, Gogebic and Ontonagon Counties, Michigan (No. 1365).

Pufahl, P.K. and Fralick, P.W., 2004. Depositional controls on Palaeoproterozoic iron formation accumulation, Gogebic range, Lake Superior region, USA. Sedimentology, 51(4), pp.791-808.

Pufahl, P.K. and Hiatt, E.E., 2012. Oxygenation of the Earth's atmosphere–ocean system: a review of physical and chemical sedimentologic responses. Marine and Petroleum Geology, 32(1), pp.1-20.

Pufahl, P.K., 1996. Stratigraphic architecture of a Paleoproterozoic iron formation depositional system: the Gunflint, Mesabi and Cuyuna iron ranges (Doctoral dissertation).

Rasmussen, B., Fletcher, I.R., Bekker, A., Muhling, J.R., Gregory, C.J. and Thorne, A.M., 2012. Deposition of 1.88-billion-year-old iron formations as a consequence of rapid crustal growth. Nature, 484(7395), pp.498-501.

Rasmussen, B., Muhling, J.R., Suvorova, A. and Krapež, B., 2016. Dust to dust: Evidence for the formation of “primary” hematite dust in banded iron formations via oxidation of iron silicate nanoparticles. Precambrian Research, 284, pp.49-63.

Reading, H.G. and Reading, H.G. eds., 1978. Sedimentary environments and facies (Vol. 60). Oxford: Blackwell.

Reed., R and Daniels, J. DNR, 1987.

Reineck, H. and Singh, IB 1980. Depositional Sedimentary Environments. New York, Springer-Verlag, Second Ed., 549 p.

Reineck, H.E. and Wunderlich, F., 1968. Classification and origin of flaser and lenticular bedding. Sedimentology, 11(1-2), pp.99-104.

Robbins, L.J., Funk, S.P., Flynn, S.L., Warchola, T.J., Li, Z., Lalonde, S.V., Rostron, B.J., Smith, A.J., Beukes, N.J., de Kock, M.O. and Heaman, L.M., 2019. Hydrogeological constraints on the formation of Palaeoproterozoic banded iron formations. Nature Geoscience, p.1.

Schmidt RG. Geology of the Precambrian W (lower Precambrian) rocks in western Gogebic County, Michigan. US Govt. Print. Off.,; 1976.

Schmidt, Robert Gordon. 1980. The Marquette Range Supergroup in the Gogebic iron district, Michigan and Wisconsin; B; 1460; U.S. Govt. Print. Off.

Schneider, D.A., Bickford, M.E., Cannon, W.F., Schulz, K.J. and Hamilton, M.A., 2002. Age of volcanic rocks and syndepositional iron formations, Marquette Range Supergroup: implications for the tectonic setting of Paleoproterozoic iron formations of the Lake Superior region. Canadian Journal of Earth Sciences, 39(6), pp.999-1012.

Schulz, Klaus J., and William F. Cannon. "The Penokean orogeny in the Lake Superior region." Precambrian Research 157.1 (2007): 4-25.

Simonson, B.M. and Hassler, S.W., 1996. Was the deposition of large Precambrian iron formations linked to major marine transgressions?. The Journal of Geology, 104(6), pp.665-676.

Simonson, B.M., 1985. Sedimentological constraints on the origins of Precambrian iron-formations. Geological Society of America Bulletin, 96(2), pp.244-252.

Sims, P.K. 1992 Geological Map of Precambrian rocks, Southern Lake superior region, Wisconsin and northern Michigan. USGS_I-2185. USGS.

Sims, P.K., Schmus, W.V., Schulz, K.J. and Peterman, Z.E., 1989. Tectono-stratigraphic evolution of the Early Proterozoic Wisconsin magmatic terranes of the Penokean Orogen. Canadian Journal of Earth Sciences, 26(10), pp.2145-2158.

Terwindt, J.H., 1971. Sand waves in the Southern Bight of the North Sea. Marine Geology, 10(1), pp.51-67.

Trent, V.A., 1973. Geologic map of the Marenisco and Wakefield NE quadrangles, Gogebic County, Michigan (No. 73-280).